Journal of Solid State Chemistry 181 (2008) 2653–2659

Contents lists available at ScienceDirect

Journal of Solid State Chemistry

journal homepage: www.elsevier.com/locate/jssc

Electronic structure and photocatalytic properties of $ABi_2Ta_2O_9$ (A = Ca, Sr, Ba)

Yingxuan Li, Gang Chen *, Hongjie Zhang, Zhonghua Li, Jingxue Sun

Department of Applied Chemistry, Harbin Institute of Technology, Harbin 150001, People's Republic of China

ARTICLE INFO

Article history:
Received 2 February 2008
Received in revised form
28 April 2008
Accepted 11 May 2008
Available online 22 May 2008

Keywords:
Photocatalyst
$ABi_2Ta_2O_9$ (A = Ca, Sr, Ba)
Water splitting
DFT calculation

ABSTRACT

A new series of layered perovskite photocatalysts, $ABi_2Ta_2O_9$ (A = Ca, Sr, Ba), were synthesized by the conventional solid-state reaction method and the crystal structures were characterized by powder X-ray diffraction. The results showed that the structure of $ABi_2Ta_2O_9$ (A = Ca, Sr) is orthorhombic, while that of $BaBi_2Ta_2O_9$ is tetragonal. First-principles calculations of the electronic band structures and density of states (DOS) revealed that the conduction bands of these photocatalysts are mainly attributable to the Ta 5*d*+Bi 6*p*+O 2*p* orbitals, while their valence bands are composed of hybridization with O 2*p*+Ta 5*d*+Bi 6*s* orbitals. Photocatalytic activities for water splitting were investigated under UV light irradiation and indicated that these photocatalysts are highly active even without co-catalysts. The formation rate of H_2 evolution from an aqueous methanol solution is about 2.26 mmol h^{-1} for the photocatalyst $SrBi_2Ta_2O_9$, which is much higher than that of $CaBi_2Ta_2O_9$ and $BaBi_2Ta_2O_9$. The photocatalytic properties are discussed in close connection with the crystal structure and the electronic structure in details.

1. Introduction

Photocatalytic splitting of water into H_2 and O_2 using oxide semiconductor powder is an attractive solution to supply clean and recyclable hydrogen energy. Layered metal oxides, such as $A_4Ta_xNb_{6-x}O_{17}$ (A = K, Rb) [1], $A_2SrTa_2O_7 \cdot nH_2O$ (A = H, K, and Rb) [2], $Sr_2Nb_2O_7$ [3,4], $KCa_2Nb_3O_{10}$ [5], and $RbLnTa_2O_7$ (Ln = La, Pr, Nd, and Sm) [6], $A_2La_2Ti_3O_{10}$ (A = K, Rb, Cs) [7,8], $A_4Nb_6O_{17}$ (A = K, Rb) [9], $K_{1-x}La_xCa_{2-x}Nb_3O_{10}$ (x = 0, 0.25, 0.5, 0.75) [10], $H_2La_{2/3}Ta_2O_7$ [11], etc., have been demonstrated to be highly active photocatalysts under light irradiation. The layered materials use their interlayer space as reaction sites, where electron–hole recombination process could be retarded by physical separation of electron and hole pairs generated by photoabsorption resulting in the higher photocatalytic activities of these layered photocatalysts for water splitting [2]. Unfortunately, the number of Ta-based photocatalysts with layered structure is still limited. A series of layered ceramics represented by $A_{m-1}Bi_2M_mO_{3m+3}$ (m = 1–4) were first synthesized by Aurivilllius [12]. It should be noted that the family of layered perovskite-type oxides have a wide variety of derivatives produced by replacing A and M sites with various metal cations. For example, when Pb was incorporated in the A site and Nb in the M site, $PbBi_2Nb_2O_9$, photocatalytic H_2 evolution under visible light irradiation ($\lambda > 420$ nm) proceeded [13,14]. $ABi_2Ta_2O_9$ (A = Ca, Sr, Ba) belong to the family of the Aurivillius-type oxides with the pseudo-perovskite layers $m = 2$. On the other hand, no photocatalytic properties of the compounds have been reported so far.

The Bi-based photocatalysts such as $BiVO_4$, and $BiMoO_6$ have been reported to be visible-light-driven photocatalysts for O_2 evolution from water containing sacrificial reagents [15,16]. Moreover, Bi_2WO_6, and $Bi_{12}TiO_{20}$ have been described as photocatalysts for degradation of organic pollutants under visible light irradiation [17,18]. Bismuth is a candidate for a valence-band-control element for the hybrid orbital of Bi 6*s* and O 2*p* [15]. Photocatalytic hydrogen production from water over photocatalysts of Bi_2O_3–Nb_2O_5 and Bi_2O_3–Ta_2O_5 systems has been less investigated and the only phases known in these systems are Bi_2MNbO_7 (M = Al, Ga, In) [19], Bi_2RNbO_7 (R = Y, rare earth) [20], Bi_2MTaO_7 (M = Ga, In, Fe) [21], $BiTa_{1-x}Nb_xO_4$ ($0 \leqslant x \leqslant 1$) [22], and $PbBi_2Nb_2O_9$ [13,14]. It is to be noted that all these phases except $PbBi_2Nb_2O_9$ and $BiTa_{1-x}Nb_xO_4$ ($0 \leqslant x \leqslant 1$) have a pyrochlore-type crystal structure. For most of the photocatalysts, it is necessary to load transition metal co-catalysts to achieve high activities for water splitting. Because these bismuth mixed oxides, $ABi_2Ta_2O_9$ (A = Ca, Sr, Ba), have the characteristic layered structures of perovskite, it would be interesting to examine the band structure and photochemical properties of them. Although these materials only respond to UV light and thus have limitation in practical hydrogen production using solar energy, it is desirable to investigate the influence of crystal and electronic structures on photocatalytic activities for water splitting. The results would help understand how to control band structure of a

* Corresponding author. Fax: +86 451 86413753.
E-mail address: gchen@hit.edu.cn (G. Chen).

0022-4596/$ - see front matter © 2008 Elsevier Inc. All rights reserved.
doi:10.1016/j.jssc.2008.05.020

semiconductor and why a material makes a good photocatalyst, which in turn could provide a guideline to select or design new and more efficient photocatalysts under UV as well as under visible light.

In this paper, a new series of photocatalysts, $ABi_2Ta_2O_9$ (A = Ca, Sr, Ba) with layered perovskite structures were synthesized and a systematic investigation on the photocatalytic and electronic properties of them were reported. The factors affecting the difference in the photocatalytic activities were investigated.

2. Experimental section

2.1. Preparation of samples

Polycrystalline samples of $ABi_2Ta_2O_9$ (A = Ca, Sr, Ba) were prepared by solid-state reaction of carbonates ($CaCO_3$, $SrCO_3$, $BaCO_3$, 99%) and oxides (Bi_2O_3 and Ta_2O_5, 99.9%). A mixture of these starting materials with an appropriate molar ratio was ground well in an agate mortar before firing. The heating schedule of $ABi_2Ta_2O_9$ (A = Ca, Sr) is based on the preparative method used for $SrBi_2Nb_2O_9$: the starting compounds were thoroughly ground and heated at 900 °C for 15 h, 1000 °C for 15 h, and 1200 °C for 24 h with intermittent grinding [23]. For $BaBi_2Ta_2O_9$, the mixture of $BaCO_3$, Bi_2O_3, and Ta_2O_5 is heated at 1000 °C for 72 h with intermediate regrinding to complete reaction [24].

2.2. Characterization

X-ray diffraction using a Rigaku D/max-2000 diffractometer equipped with Cu$K\alpha$ radiation ($\lambda = 0.15406$ nm) was carried out for the sintered samples at room temperature. The 2θ range was $10^\circ \leqslant 2\theta \leqslant 90^\circ$ with increment of 0.02°. The infrared spectrum was recorded by a Perkin-Elmer Spectrum and a KBr-disc technique. Diffuse reflectance spectra were measured on a UV–vis spectrophotometer (TU-1900). The surface area was measured by the BET method (ST-2000).

The plane-wave-based density functional theory (DFT) calculation was based on the full-potential linear-muffin-tin-orbital (FP-LMTO) method [25,26]. The electronic exchange-correlation energy was treated within the framework of the generalized gradient approximation (GGA) PW91, an improvement of the local spin density approximation (LSDA) within DFT that is known to be an efficient and accurate scheme for solving the many-electron problem of a crystal [26,27]. The core electrons were replaced with ultrosoft norm-conserving pseudopotential, and the O $2s^2 2p^4$, Bi $6s^2 6p^3$, Ca $3s^2 3p^6 4s^2$, Sr $4s^2 4p^6 5s^2$, Ba $5s^2 5p^6 6s^2$, and Ta $5d^3 6s^2$, electrons were treated explicitly. The kinetic energy cut-off was set at 260 eV, and the unit cell includes $(ABi_2Ta_2O_9)_2$ structure. The crystallographic parameters including lattice parameters and atomic positions were adopted from the literature for the calculation [28]. The system structures were optimized by first-principle calculations.

2.3. Photocatalytic reactions

The photocatalytic gas evolution from aqueous solutions of methanol was conducted in an outer irradiation quartz cell, which was connected to a closed gas-circulating system. The H_2 evolution reaction was performed in an aqueous CH_3OH/H_2O solution (0.2 g powder catalyst, 50 mL CH_3OH, 350 mL deionized H_2O), and the O_2 evolution reaction was performed in $AgNO_3$ solution (0.2 g powder catalyst, 10 mmol $AgNO_3$, 400 mL deionized H_2O). The reaction was carried out by irradiating the mixture with light from a 350 W Hg lamp. Gas evolution was analyzed by a gas chromatograph (Agilent 6820, TCD, Ar carrier).

3. Results and discussion

3.1. Structure and infrared spectroscopy

Fig. 1 shows X-ray diffraction patterns of compounds $ABi_2Ta_2O_9$ (A = Ca, Sr, Ba). With the increasing of the ionic radii of A (from Ca to Sr to Ba), not only lattice parameters but also crystal structure types of the materials changed. The X-ray diffraction patterns of $ABi_2Ta_2O_9$ (A = Ca, Sr) were indexed based on an orthorhombic lattice with the $A2_1am$ space group by using the JCPDS PDF database (PDF#49-0608), indicating that those compounds consist of a single phase. The lattice parameters of $CaBi_2Ta_2O_9$ and $SrBi_2Ta_2O_9$ were determined to be $a = 0.5467$ nm, $b = 0.5427$ nm, $c = 2.4931$ nm and $a = 0.5473$ nm, $b = 0.5527$ nm, $c = 2.5031$ nm, respectively. The lattice parameters increased as the size of the A-site cation increased. As shown in Fig. 1(b), when Sr^{2+} was replaced by Ca^{2+}, the corresponding diffraction peaks are shifted toward higher diffraction angles, indicating an increase in the lattice parameters of these materials, which is in agreement with the result mentioned above. As reported [24,28,29], the diffraction patterns for $BaBi_2Ta_2O_9$ can be indexed to a tetragonal cell with space group $I4/mmm$. The lattice constants are determined to be $a = 0.3954$ nm and $c = 2.5487$ nm.

Fig. 2(a) and (b) represent the schematic crystal structure of $BaBi_2Ta_2O_9$ and $ABi_2Ta_2O_9$ (A = Ca, Sr), respectively. The three oxides as members of the $(Bi_2O_2)^{2+}$ $(A_{m-1}M_mO_{3m+1})^{2-}$ family of compounds with $m = 2$ consist of $(Bi_2O_2)^{2+}$ layers interleaved with $(AM_2O_7)^{2-}$ perovskite-type layers. In the prototype structure,

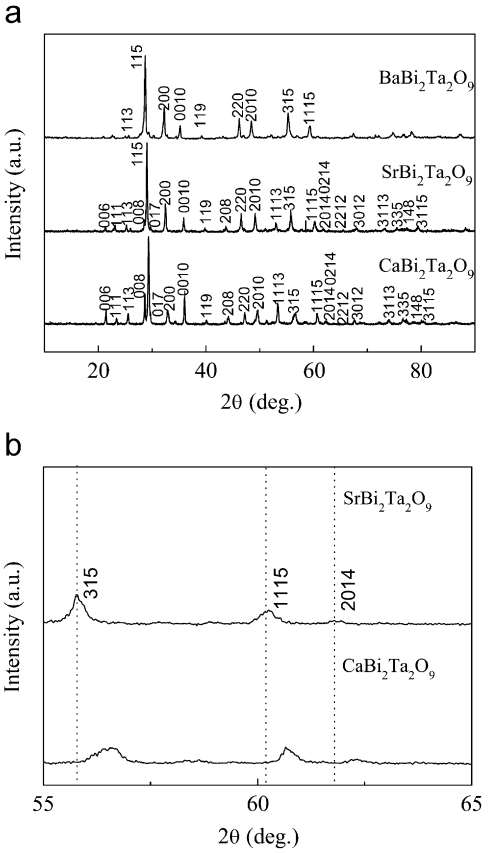

Fig. 1. X-ray diffraction patterns for the Auruvillius-tupe oxides $ABi_2Ta_2O_9$ (A = Ca, Sr, Ba).

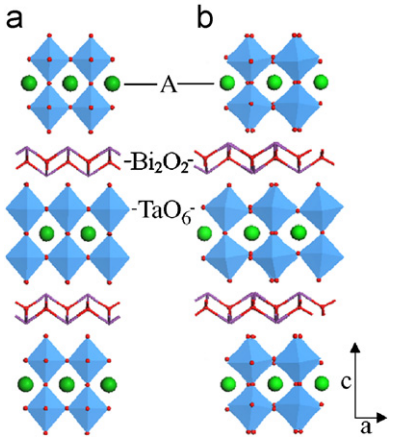

Fig. 2. Schematic crystal structure of $ABi_2Ta_2O_9$ (A = Ca, Sr, Ba): (a) $BaBi_2Ta_2O_9$ and (b) $ABi_2Ta_2O_9$ (A = Ca, Sr).

A is coordinated to 12 oxygen atoms, bismuth is bonded to 4 oxygen atoms in a square pyramidal geometry, while tantalum occupy the TaO_6 position in the perovskite layer [23]. The orthorhombic space group $A2_1am$, which may be considered as derived from an archetypal parent phase, space group $I4/mmm$, by polar displacements of the A cation and co-operative tilting of the TaO_6 octahedral units. In the perovskite-type unit of $ABi_2Ta_2O_9$ (A = Ca, Sr), with the orthorhombic structure, the TaO_2 plane is under compressive stress while the AO plane is under tensile stress, which causes co-operative rotations of TaO_6 octahedra [28]. In the Bi-layered compounds, however, such cooperative rotations of the octahedra are not allowed owing to the presence of the Bi_2O_2 layers above and below the ATa_2O_7 perovskite-type unit: thus, the octahedron itself is considerably distorted, leading to the $A2_1am$ orthorhombic symmetry [28]. For $BaBi_2Ta_2O_9$, the bigger size of Ba atom causes the smaller compressive stress in the perovskite unit [28]. As a result, the mismatch between the perovskite-layer and the Bi_2O_2 layer is reduced, leading to much smaller distortion in the TaO_6 octahedra [30]. This difference in crystal structure might lead to different photocatalytic behavior of the compounds.

The IR spectra of the investigated materials are shown in Fig. 3. All samples show characteristic vibration bands between 450 and 1000 cm^{-1}, which are due to Sr–O (or Ca–O, Ba–O), Bi–O, and Ta–O vibrations [31]. As shown in Fig. 3, the bandwidths and positions are quite similar from one compound to the next, but small variations and shifts are present. Therefore, it can be inferred from IR spectra that the three compounds have similar structural models, in agreement with the result getting from X-ray diffraction patterns. Considering the difference in A site of $ABi_2Ta_2O_9$ (A = Ca, Sr, Ba) oxides, the exact positions of corresponding atoms may differ slightly. Affected by the small difference of atomic positions, the force constant of the vibrational modes varies, thus brings the small shifts in vibrational frequency. The IR spectra also show that there are slight differences in crystal structures of $ABi_2Ta_2O_9$ (A = Ca, Sr, Ba) compounds.

3.2. UV–vis diffuse reflectance spectra

It is important to study the optical absorption of the samples because the UV–vis absorption edge is relevant to the energy band of semiconductor catalyst. UV–vis diffuse reflectance spectra of $ABi_2Ta_2O_9$ (A = Ca, Sr, Ba) are shown in Fig. 4. The reflectivity spectrum was transformed to absorbance intensity through Kubelka–Munk method. It can be seen that the semiconductors

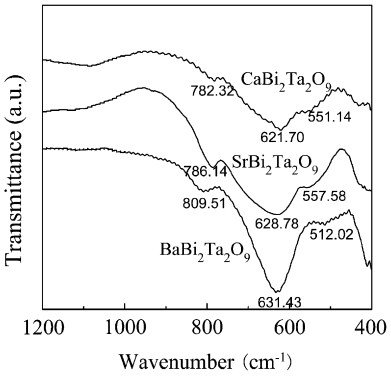

Fig. 3. IR spectra for the photocatalysts $ABi_2Ta_2O_9$ (A = Ca, Sr, Ba).

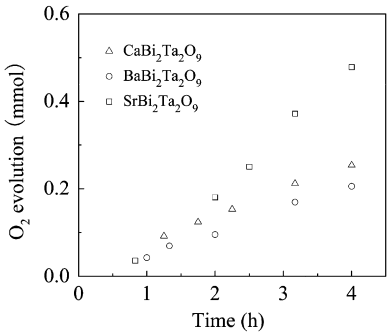

Fig. 4. UV–vis diffuse reflectance spectra for the semiconductors $ABi_2Ta_2O_9$ (A = Ca, Sr, Ba).

have a steep absorption edge, indicating that their absorption relevant to the band gap is due to the intrinsic transition of these semiconductors and not from the transition from impurity levels [32], which is in good agreement with the band calculations described below. As can be seen in Fig. 4, the absorption onsets shifted continuously from longer to shorter wavelength as the cation radius in the A site of $ABi_2Ta_2O_9$ (A = Ca, Sr, Ba) samples decreased. The absorption characteristics of $CaBi_2Ta_2O_9$ were quite similar to that of $SrBi_2Ta_2O_9$ except for slightly shorter onset wavelength and the band gaps of $CaBi_2Ta_2O_9$ and $SrBi_2Ta_2O_9$ samples estimated from the onsets of the diffuse reflection spectra are 3.67 and 3.64 eV, respectively. On the other hand, the estimated band gap of $BaBi_2Ta_2O_9$ with tetragonal structure is 3.52 eV, which is smaller than those of $CaBi_2Ta_2O_9$ and $SrBi_2Ta_2O_9$ with orthorhombic structure. Moreover, the result is in good agreement with the conclusion derived from the DFT electronic structure calculations.

3.3. Photocatalytic activities

The photocatalytic decomposition of water on these catalysts without any loaded metals was carried out in order to clarify the relationship between the crystal structure and the photocatalytic activities of $ABi_2Ta_2O_9$ (A = Ca, Sr, Ba). In our experiments, the sacrificial reagent methanol was employed to evaluate the photocatalytic activities of these photocatalysts. The time dependence of the amount of hydrogen evolution on $ABi_2Ta_2O_9$ (A = Ca, Sr, Ba) in an aqueous CH_3OH/H_2O solution is shown in Fig. 5. During the experimental period, H_2 evolution increased linearly. As shown in Fig. 5, photocatalyst $SrBi_2Ta_2O_9$ shows much higher activity in evolving H_2 than $CaBi_2Ta_2O_9$ and $BaBi_2Ta_2O_9$ under UV light irradiation. For the $SrBi_2Ta_2O_9$ photocatalyst, the total amount of the H_2 evolved in the first 9 h is more than 20 mmol,

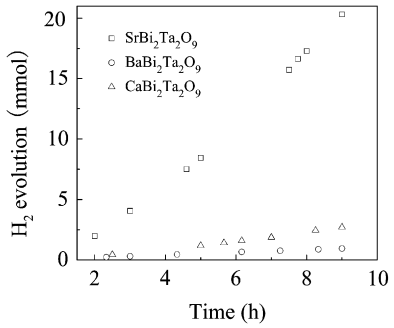

Fig. 5. Amount of H_2 evolved vs. irradiation time on $ABi_2Ta_2O_9$ (A = Ca, Sr, Ba) under UV light irradiation in CH_3OH/H_2O solution (cat.: 0.2 g, CH_3OH: 50 mL, H_2O: 350 mL, and Hg lamp: 350 W, outer irradiation).

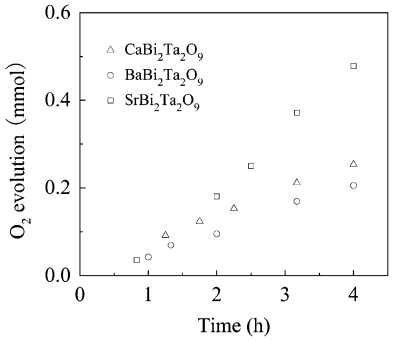

Fig. 6. Amount of O_2 evolved vs. irradiation time from the $AgNO_3/H_2O$ solution under UV light irradiation for the photocatalysts $ABi_2Ta_2O_9$ (A = Ca, Sr, Ba) (cat.: 0.2 g, $AgNO_3$: 10 mmol, H_2O: 400 mL, and Hg lamp: 350 W, outer irradiation).

indicating a formation rate of 2.26 mmol h^{-1}. However, for the $CaBi_2Ta_2O_9$ and $BaBi_2Ta_2O_9$ photocatalysts, the total amounts of the H_2 evolved in the first 9 h are much less than that for the $SrBi_2Ta_2O_9$ photocatalyst, with H_2 evolution rates of 0.30 and 0.11 mmol h^{-1}, respectively. It is noteworthy that these Aurivillius-type oxides, especially $SrBi_2Ta_2O_9$, show such high activities without co-catalysts such as platinum. This means that the Auruvillius-type oxides possess good catalytic sites and sufficiently high conduction band levels for H_2O reduction to form H_2.

For photocatalytic water splitting, the conduction band level should be more negative than the reduction potential of H_2O to form H_2 and the valence band should be more positive than the oxidation potential of H_2O to form O_2. In order to make sure whether the position of valence band of these photocatalysts is lower than that of O_2/H_2O or not, $AgNO_3$ was used as electron acceptor for the photocatalytic oxidation of water. The activities of O_2 evolution from an aqueous $AgNO_3$ (10 mmol $AgNO_3$, 400 mL deionized H_2O) solution over the $ABi_2Ta_2O_9$ (A = Ca, Sr, Ba) powder catalysts (0.2 g) under Hg lamp irradiation are shown in Fig. 6. The O_2 evolution increased with illumination time, as did H_2 evolution. The rates of the O_2 evolution were 0.12, 0.06, and 0.05 mmol h^{-1} in the 4 h reaction for $SrBi_2Ta_2O_9$, $CaBi_2Ta_2O_9$, and $BaBi_2Ta_2O_9$, respectively. The above results indicate that the $ABi_2Ta_2O_9$ (A = Ca, Sr, Ba) semiconductors have suitable band structure for the reduction of H^+ to H_2 and oxidation of H_2O to O_2, respectively. But there is no hydrogen evolution is observed when no any hole scavenger is existed in solution. This phenomenon is often observed in water splitting over semiconductor photocatalysts and has been interpreted as the difficulty of O_2 formation and the rapid reverse reaction between H_2 and O_2 [4].

It is known that the photocatalytic activity of a semiconductor is dominated by many factors, such as the crystal structures, electronic structures, surface area, and so on. The difference in the surface area of the photocatalysts can generally lead to the difference in photocatalytic activity since an efficient photocatalytic reaction process occurs on the photocatalyst surface. As shown in Table 1, $ABi_2Ta_2O_9$ (A = Ca, Sr, Ba) have very similar surface area; hence the difference in photocatalytic activity cannot be mainly attributed to variations in surface area. The fact suggests that it may be mainly due to the different crystal and electronic structures.

Table 1
Photocatalytic activities of the photocatalysts $CaBi_2Ta_2O_9$, $SrBi_2Ta_2O_9$, $BaBi_2Ta_2O_9$

Catalyst	Band gap (eV)	Surface area ($m^2 g^{-1}$)	Activity (mmol h^{-1})	
			H_2[a]	O_2[b]
$CaBi_2Ta_2O_9$	3.67	1.96	0.30	0.06
$SrBi_2Ta_2O_9$	3.64	2.36	2.26	0.12
$BaBi_2Ta_2O_9$	3.52	2.18	0.11	0.05

[a] Catalyst: 0.2 g, reactant solution: CH_3OH: 50 mL, H_2O: 350 mL, 350 W Hg lamp outer irradiation.
[b] Reactant solution: $AgNO_3$: 10 mmol, H_2O: 400 mL, 350 W Hg lamp outer irradiation.

A photocatalysis reaction to split water with oxide semiconductor includes: (i) adsorption of photons corresponding to the energy band gap of the material, leading to generation of electron–hole pairs in the semiconductor particles, (ii) migration of photogenerated carriers to the surfaces of particles, reduction and oxidation of surface-adsorbed water by them to produce H_2 and O_2, respectively. The former is controlled by the energy band structure of a semiconductor, while the latter is strongly relevant to the crystal structure of the semiconductor.

$SrBi_2Ta_2O_9$ and $CaBi_2Ta_2O_9$ have similar layered perovskite structures in which TaO_6 octahedra are connected by corner sharing as shown in Fig. 2. The study on influence of crystal structure on luminescent properties has concluded that the closer the bond angle of M–O–M is to the ideal 180° the more the excitation energy is delocalized [21]. This means that the bond angle of M–O–M is one of the important factors affecting the photocatalytic and photophysical properties of semiconductors. For $ABi_2Ta_2O_9$ (A = Ca, Sr), the bond angle of Ta–O–Ta increases with increasing A^{2+} cation size [28,33], in agreement with the result getting from the optimized structures by first-principle calculations. The bond angles under the optimized structures of Ta–O–Ta in $SrBi_2Ta_2O_9$ and $CaBi_2Ta_2O_9$ are 152.313°, and 145.382°, respectively. This suggests that although $ABi_2Ta_2O_9$ (A = Ca, Sr) have similar crystal structure, photogenerated electron–hole pairs might move more easily when the bond angle of Ta–O–Ta is larger. The mobility of electron–hole pairs affects the photocatalysis because it affects the probability of electrons and holes to reach reaction sites on the surface of photocatalyst [16]. Therefore, the bond angle of Ta–O–Ta might be one of the factors for the much higher activity of $SrBi_2Ta_2O_9$ than that of $CaBi_2Ta_2O_9$.

For the photocatalytic water splitting, charge separation is necessary to prevent recombination of the photo-induced electrons and holes. The migration of charge carriers to the surface of the semiconductor is quite complicated. The lattice distortion is one of the important parameters for charge separation, and contributes to an increase in the photocatalytic activity [34,35]. In the $A2_1am$ orthorhombic structure, atomic displacements along the a-axis from the corresponding positions in the parent tetragonal structure is observed. No ions in pseudotetragonal $BaBi_2Ta_2O_9$ are displaced in such ways [28]; thus, the lattice distortion in orthorhombic structure might be one reason for the higher activities of the $ABi_2Ta_2O_9$ (A = Ca, Sr) than $BaBi_2Ta_2O_9$ with tetragonal structure. For $ABi_2Ta_2O_9$ (A = Ca, Sr) with orthorhombic structure, the displacements along the a-axis show

that the Bi_2O_2 layers and the ATa_2O_7 perovskite-type units shift in opposite directions and the Bi^{3+} ion in the Bi_2O_2 layer is more displaced in $SrBi_2Ta_2O_9$ than that in $CaBi_2Ta_2O_9$ [28]. Thus, this larger lattice distortion also contributes to much higher activity of $SrBi_2Ta_2O_9$ than that of $CaBi_2Ta_2O_9$. Based on the results mentioned above, it is rationally assumed that $SrBi_2Ta_2O_9$ has the most suitable crystal structure for photocatalytic water splitting in the $ABi_2Ta_2O_9$ (A = Ca, Sr, Ba) photocatalysts, although $ABi_2Ta_2O_9$ (A = Ca, Sr) have the same orthorhombic structure. It is generally agreed that a slight modification of the structure of a semiconductor has a dramatic effect on the concentration and mobility of charge [36], which directly affect the photocatalytic properties of the semiconductors. Therefore, it is reasonable for $SrBi_2Ta_2O_9$ to show much higher photocatalytic activity than $ABi_2Ta_2O_9$ (A = Ca, Ba).

3.4. Electronic structure calculation

The calculated band structures of $ABi_2Ta_2O_9$ (A = Ca, Sr, Ba) are shown in Fig. 7. The Fermi energy, defined as the highest occupied energy level, has been taken as the valence band maximum (VBM). Both the valence band maximum and the conduction band minimum (CBM) of the $ABi_2Ta_2O_9$ (A = Ca, Sr) were found along Y point to G point. This means that the compounds are direct-gap semiconductor materials. For $BaBi_2Ta_2O_9$, the VBM is located along X point to P point, while the CBM lies at the G point, indicating that it is an indirect-gap semiconductor. The direct band gap is one of the desirable properties of photocatalyst materials because light absorption for this kind of materials can occur more efficiently in comparison to that for materials with the indirect band gap [37]. Therefore, the change from direct-gap to indirect-gap semiconductor material might be one of the factors for the lower photocatalytic activities of $BaBi_2Ta_2O_9$ than $ABi_2Ta_2O_9$ (A = Ca, Sr). It can be seen from Fig. 7 that the width of the energy gaps of the $CaBi_2Ta_2O_9$, $SrBi_2Ta_2O_9$, and $BaBi_2Ta_2O_9$ are 2.4, 2.1, and 1.2 eV, respectively. With the variation of the ionic radius of Ba^{2+}, Sr^{2+}, and Ca^{2+}, the band gaps of these compounds change periodically, which is in good agreement with the band

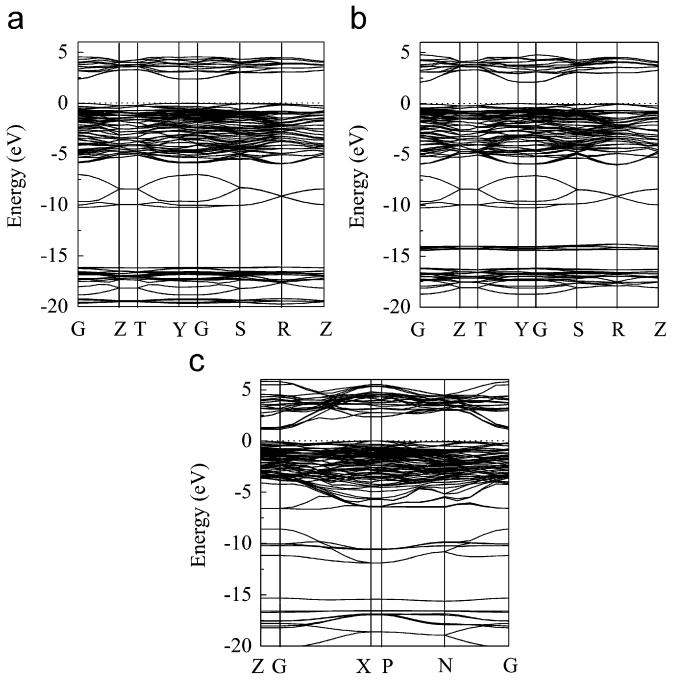

Fig. 7. The calculated band structures of $ABi_2Ta_2O_9$ (A = Ca, Sr, Ba): (a) $CaBi_2Ta_2O_9$, (b) $SrBi_2Ta_2O_9$ and (c) $BaBi_2Ta_2O_9$.

gap estimated from onsets of diffuse reflectance spectra. The increase in the band gap from $SrBi_2Ta_2O_9$ to $CaBi_2Ta_2O_9$ stems from the strong hybridizations between Ta 5*d* and O 2*p* orbits [30]. Our calculated result of $SrBi_2Ta_2O_9$ is in good agreement with the previously calculated result [38]. The calculated band gaps are smaller than that obtained experimentally, which is pointed out as a common feature of DFT calculations. This underestimation comes from some flaws in the GGA used for this calculation [39].

Fig. 8 shows the total density of states (TDOS) and partial density of states (PDOS), corresponding to the energy region in Fig. 7. The top of valence band is set to be zero on the ordinate. The band gap exists in the band structure. The total DOS of $BaBi_2Ta_2O_9$ are different from those of $CaBi_2Ta_2O_9$, and $SrBi_2Ta_2O_9$, which agrees well with the reports in Ref. [30]. This difference in electronic structure might be caused by the difference between orthorhombic and tetragonal structure because the crystal field can greatly influence the orbital distribution of the atoms [32]. The TDOS of $CaBi_2Ta_2O_9$, and $SrBi_2Ta_2O_9$ exhibit a sharp raise near the edges of both valence and conduction bands, reflecting a larger number of effective states available for the photo-induced electrons and holes [40]. This would somehow contribute to the higher photocatalytic activities of $CaBi_2Ta_2O_9$, and $SrBi_2Ta_2O_9$ than that of $BaBi_2Ta_2O_9$. From the PDOS of Ca (or Sr or Ba), we can see that the contribution of Ca (or Sr or Ba) orbitals to the valence and conduction bands is negligibly small. There are a few single bands around −10 eV in Fig. 8. This can be assigned that these bands consist of Bi 6*s* and O2 2*s* orbitals which belong to the $(Bi_2O_2)^{2+}$ planes. The very small dispersion of these bands implies its localized character. The next higher bands, ranging from about −6 eV up to the Fermi level, are valence bands. Although the valence band presents mainly O 2*p* character, there is quite strong hybridization with Bi 6*s* and Ta 5*d* orbitals, as is evident from the DOS shown in Fig. 8. The Ta 5*d* contribution is zero at the valence band maximum but rises strongly with decreasing binding energy and the hybridization of Ta 5*d*–O 2*p* leading to charge transfer from O back to Ta 5*d* makes the bonds covalent. At the top of the valence band, the Bi 6*s* orbitals mix more strongly with the O 2*p* orbitals, which is a characteristic feature for the oxide materials containing bismuth. The Bi contribution has *s*- and *p*-like characters, corresponding mainly to the upper part of the valence band and the lower part of the valence band, respectively. These contributions arise from a strong hybridization between O 2*p* valence band states with Bi 6*s* (fully occupied) and Bi 6*p* (conduction) bands [41]. The conduction bands of the materials consisted of Bi 6*p*, Ta 5*d* and O 2*p* orbitals but the bottom of conduction band is mainly determined by Ta 5*d* state rather than the Bi 6*p* and O 2*p* orbitals. The recent findings that typical d^{10} metal oxides become strong photocatalysts for water decomposition are explained in terms of the advantages of sp orbitals with a large dispersion in the conduction bands [42]. It is clearly seen from Fig. 8 that the Ta 5*d*, Bi 6*p*, and O 2*p* states overlap in the conduction band. Therefore, the density-of-states distribution of Bi 6*p*, and O 2*p* states in the conduction band is helpful for a better photocatalytic performance of the Aurivillius-type oxides.

3.5. Band structure model

Band structure control is necessary in order to develop new photocatalysts for splitting water into H_2 under visible light irradiation. The band structures of $ABi_2Ta_2O_9$ (A = Ca, Sr, Ba) can be roughly described as shown in Fig. 9. In accordance with DFT electronic structure calculations, the valence band is consisted of O 2*p*, Ta 5*d* and Bi 6*s* orbitals and the conduction band is from Bi 6*p*, Ta 5*d* and O 2*p* orbitals. Although, as shown in Fig. 4, these photocatalysts do not have the ability to respond to the

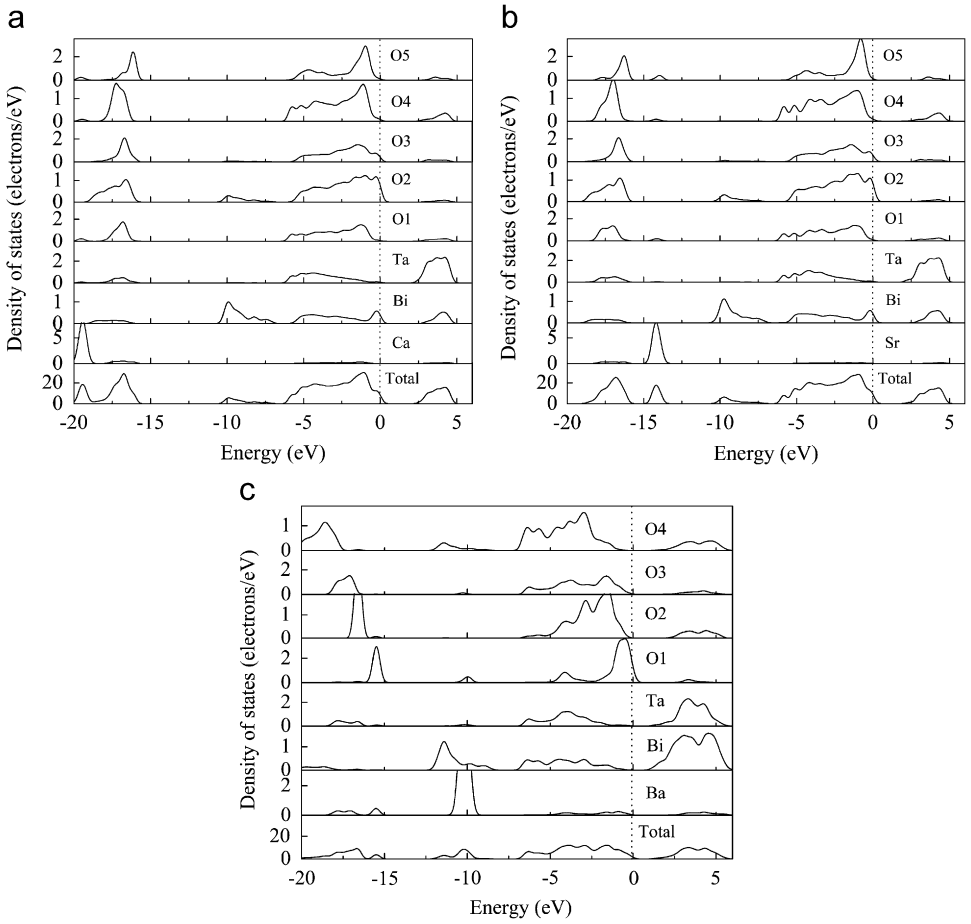

Fig. 8. The density of states (DOS) of $ABi_2Ta_2O_9$ (A = Ca, Sr, Ba): (a) $CaBi_2Ta_2O_9$, (b) $SrBi_2Ta_2O_9$ and (c) $BaBi_2Ta_2O_9$.

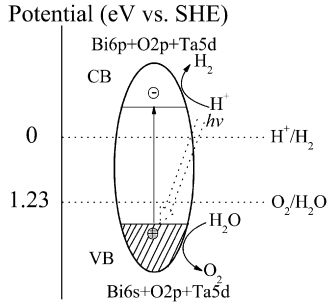

Fig. 9. Band structures of $ABi_2Ta_2O_9$ (A = Ca, Sr, Ba).

Table 2
Band gaps of $ABi_2Ta_2O_9$, ATa_2O_6 (A = Ca, Sr, Ba), and $Sr_2Ta_2O_7$

Catalyst	Band gap (eV)
$CaBi_2Ta_2O_9$	3.67
$SrBi_2Ta_2O_9$	3.64
$BaBi_2Ta_2O_9$	3.52
$CaTa_2O_6$[a]	4.0
$SrTa_2O_6$[a]	4.4
$BaTa_2O_6$[a]	4.1
$Sr_2Ta_2O_7$[b]	4.6

[a] From Ref. [43]
[b] From Ref. [34]

wavelength in the visible light region ($\lambda > 420$ nm), the band gaps are much narrower than the photocatalysts without bismuth such as ATa_2O_6 (A = Ca, Sr, Ba) [43] and $Sr_2Ta_2O_7$ [34] (Table 2). As for tantalates, a typical semiconductor photocatalysts locating in d block possessing d^0 electronic configuration, usually their conduction bands and valence bands are mainly consisting of Ta 5d and O 2p orbitals, respectively. However, for the metal oxides containing bismuth, an additional hybridization of the occupied Bi 6s and O 2p orbital seem to result in a narrower band gap. This hybridization would push up the position of the valence band giving the smaller band gap compared to their respective bismuth-free counterparts. According to the above analysis, it can be speculated that the narrower band gaps of $ABi_2Ta_2O_9$ (A = Ca, Sr, Ba) should result from the high chemical potential of Bi 6s contributable to the formation of their valence bands.

4. Conclusion

$ABi_2Ta_2O_9$ (A = Ca, Sr, Ba) with the layered perovskite structure have been synthesized by the solid-state reaction process and were found to be new photocatalysts for water splitting even in the absence of a co-catalyst. The difference in their photocatalytic activities is ascribed to their special crystal and electronic structures. The crystal structures of $ABi_2Ta_2O_9$ (A = Ca, Sr, Ba) changed with increasing ionic radius of the A^{3+} ion. $SrBi_2Ta_2O_9$ showed much higher activity since it has the most suitable crystal structure for photocatalytic water splitting in the $ABi_2Ta_2O_9$ (A = Ca, Sr, Ba) photocatalysts. The orthorhombic $ABi_2Ta_2O_9$ (A = Ca, Sr) have several advantages over the tetragonal $BaBi_2Ta_2O_9$ in photocatalytic water splitting. In the aspect of electronic structure, the direct band gap of $ABi_2Ta_2O_9$ (A = Ca, Sr) is one of

the desirable properties of photocatalyst materials and the orthorhombic phase was found to have a larger number of effective states available for the photo-induced electrons and holes. As to crystalline structure, lattice distortion may play an important role in the photogenerated charge separation, thus affecting the photocatalytic activity. It was also found that bismuth is the element that makes an essential contribution to the small band gap energy of these photocatalysts, which is noteworthy information to design new visible-light-driven photocatalysts.

Acknowledgements

This work was supported by the National Nature Science Foundation of China (20571019), the Project-sponsored by SRF for ROCS, HLJ (LC06C13) and Project-Sponsored by Program of Harbin Subject Chief Scientist (2006RFXXG001).

References

[1] K. Sayama, H. Arakawa, K. Domen, Catal. Today 28 (1996) 175–182.
[2] K. Shimizu, Y. Tsuji, T. Hatamachi, K. Toda, T. Kodama, M. Sato, Y. Kitayama, Phys. Chem. Chem. Phys. 6 (2004) 1064–1069.
[3] G.K. Hyun, W.H. Dong, K. Jindo, G.K. Young, S.J. Lee, Chem. Commun. 999 (1999) 1077–1078.
[4] W.H. Dong, H.G. Kim, J. Kim, K.Y. Cha, Y.G. Kim, J.S. Lee, J. Catal. 193 (2000) 40–48.
[5] Y. Ebina, A. Tanaka, J.N. Kondo, K. Domen, Chem. Mater. 8 (1996) 2534–2538.
[6] M. Machida, J. Yabunaka, T. Kijima, Chem. Mater. 12 (2000) 812–817.
[7] T. Takata, Y. Furumi, K. Shinohara, A. Tanaka, M. Hara, J.N. Kondo, K. Domen, Chem. Mater. 9 (1997) 1063–1064.
[8] T. Takata, K. Shinohara, A. Tanaka, M. Hara, J.N. Kondo, K. Domen, J. Photochem. Photobiol. A 106 (1997) 45–49.
[9] A. Kudo, A. Tanaka, K. Domen, K. Maruya, K. Aika, T. Onishi, J. Catal. 111 (1988) 67–76.
[10] K. Domen, Y. Ebina, S. Ikeda, A. Tanaka, J.N. Kondo, K. Maruya, Catal. Today 28 (1996) 167–174.
[11] K. Shimizu, S. Itoh, T. Hatamachi, T. Kodama, M. Sato, K. Toda, Chem. Mater. 17 (2005) 5161–5166.
[12] B. Aurivillius, Ark. Kemi. 1 (1949) 463–480.
[13] H.G. Kim, D.W. Hwang, J.S. Lee, J. Am. Chem. Soc. 126 (2004) 8912–8913.
[14] H.G. Kim, O.S. Becker, J.S. Jang, S.M. Ji, P.H. Borseb, J.S. Lee, J. Solid State Chem. 179 (2006) 1214–1218.
[15] A. Kudo, K. Omori, H. Kato, J. Am. Chem. Soc. 121 (1999) 11459–11467.
[16] Y. Shimodaira, H. Kato, H. Kobayashi, A. Kudo, J. Phys. Chem. B 110 (2006) 17790–17797.
[17] H. Fu, C. Pan, W. Yao, Y. Zhu, J. Phys. Chem. B 109 (2005) 22432–22439.
[18] J. Zhou, Z. Zou, A.K. Ray, X.S. Zhao, Ind. Eng. Chem. Res. 46 (2007) 745–749.
[19] Z. Zou, J. Ye, H. Arakawa, Chem. Phys. Lett. 333 (2001) 57–62.
[20] Z. Zou, J. Ye, H. Arakawa, J. Phys.Chem. B 106 (2002) 517–520.
[21] J. Wang, Z. Zou, J. Ye, J. Phys. Chem. Solids 66 (2005) 349–355.
[22] Z. Zou, J. Ye, K. Sayama, H. Arakawa, Chem. Phys. Lett. 343 (2001) 303–308.
[23] Ismunandar, B.J. Kennedy, Gunawan, Marsongkohadi, J. Solid State Chem. 126 (1996) 135–141.
[24] S.R. Dhagea, R. Pasricha, A.V. Muruganb, V. Ravia, Mater. Chem. Phys. 98 (2006) 344–346.
[25] O.K. Andersen, Phys. Rev. B 13 (1975) 3060–3083.
[26] N. Zhou, G. Chen, H.Z. Xian, H.J. Zhang, Mater. Res. Bull. (2007).
[27] S. Ouyang, H. Zhang, D. Li, T. Yu, Ji. Ye, Z. Zou, J. Phys.Chem. B 110 (2006) 11677–11682.
[28] Y. Shimakawa, Y. Kubo, Y. Nakagawa, S. Goto, T. Kamigama, H. Asano, Phys. Rev. B 61 (2000) 6559–6564.
[29] C. Lu, C. Wen, Mater. Lett. 38 (1999) 278–282.
[30] M.Q. Cai, Z. Yin, M.S. Zhang, Solid State Commun. 133 (2005) 663–666.
[31] H. Wang, J. Liu, M. Zhu, B. Wang, H. Yan, Mater. Lett. 57 (2003) 2371–2374.
[32] J. Wang, J. Ye, J. Mater. Chem. 15 (2005) 4246–4251.
[33] R. Macquart, B.J. Kennedy, Y. Shimakawa, J. Solid State Chem. 160 (2001) 174–177.
[34] A. Kudo, H. Kato, S. Nakagawa, J. Phys. Chem. B 104 (2000) 571–575.
[35] Y. Inoue, M. Kohno, S. Ogura, K. Sato, Chem. Phys. Lett. 267 (1997) 72–76.
[36] J. Tang, Z. Zou, J. Yin, J. Ye, Chem. Phys. Lett. 382 (2003) 175–178.
[37] D.W. Hwang, J.S. Lee, W. Li, S.H. Oh, J. Phys. Chem. B 107 (2003) 4963–4970.
[38] K. Miura, et al., J. Korean Phys. Soc. 42 (2003) 1244–1247.
[39] J.W. Liu, G. Chen, Z.H. Li, Z.G. Zhang, J. Solid State Chem. 179 (2006) 3704–3708.
[40] C. Hu, H. Teng, Appl. Catal. A: Gen. 331 (2007) 44–50.
[41] M.G. Stachiotti, C.O. Rodriguez, D.C. Ambrosch, N.E. Christensen, Phys. Rev. B 61 (2000) 14434–14439.
[42] H. Kadowaki, N. Saito, H. Nishiyama, H. Kobayashi, Y. Shimodaira, Y. Inoue, J. Phys. Chem. C 111 (2007) 439–444.
[43] A. Kudo, Catal. Surv. Asia 7 (2003) 31–38.